Multitarget Tracking Using Multiple Bistatic Range Measurements with Probability Hypothesis Densities

Martin Tobias and Aaron D. Lanterman

School of Electrical and Computer Engineering
Georgia Institute of Technology
Atlanta, Georgia 30332–0250 U.S.A.

ABSTRACT

Ronald Mahler's Probability Hypothesis Density (PHD) provides a promising framework for the passive coherent location of targets observed via multiple bistatic radar measurements. We consider tracking targets using only range measurements from a simple non-directional receiver that exploits non-cooperative FM radio transmitters as its "illuminators of opportunity." A target cannot be located at a single point by a particular transmitter-receiver pair, but rather it is located along a bistatic range ellipse determined by the position of the target relative to the receiver and transmitter. Target location is resolved by using multiple transmitter-receiver pairs and locating the target at the intersection of the resulting bistatic ellipses. Determining the intersection of these bistatic range ellipses and resolving the resultant ghost targets is generally a complex task. However, the PHD provides a convenient and simple means of fusing together the multiple range measurements to locate targets. We incorporate signal-to-noise ratios, probabilities of detection and false alarm, and bistatic range variances into our simulation.

Keywords: Multitarget Tracking, Probability Hypothesis Density, Passive Radar, Sensor Fusion, Passive Coherent Location

1. INTRODUCTION

In Ref. 1 we presented an initial application of a Probability Hypothesis Density (PHD) based particle filter to multitarget tracking using passive radar. We now consider range-only measurements and modify our simulation to match a potential real-world scenario. Realistic transmitter, receiver, and target parameters are incorporated into our simulation, and the corresponding Signal-to-Noise ratios (SNR) and probabilities of Detection (p_D) are computed. We also modify the particle-filter initialization and introduce a new method for placing birth-particles, which are used to model target entry into the radar Field of View (FoV).

We introduce the concept of passive coherent location in Sec. 2, and Sec. 3 provides a description of the bistatic radar configuration used. Our PHD particle filter implementation is the subject of Sec. 4, and a summary of the SNR, p_D, and sensor likelihood function used is provided in Sec. 5. Simulation results, an explanation of the importance of high SNR, and a description of a new birth particle method are presented in Sec. 6. Section 7 contains our conclusions and lists future work.

2. PASSIVE COHERENT LOCATION (PCL)

A bistatic radar, consisting of a passive receiver and an independent transmitting antenna, provides the following range measurement observations:

$$R_{observed} = R_T + R_R \tag{1}$$

where R_T is the distance from target to transmitter, and R_R is the distance from target to receiver. Hence, a target can be located along an ellipse, where the receiver and transmitter are located at the foci of the ellipse.

It is difficult to build highly directional receiver antennas that operate at the low frequencies of interest in a passive radar system exploiting FM broadcasts. Hence, rather than trying to exploit angle-of-arrival information, we are interested in resolving a target's location by employing multiple transmitter-receiver pairs. This allows the target to be tracked at the intersection of the resulting bistatic range ellipses. Figure 2(a) and Fig. 3 contain examples of these ellipses.

E-mail: mtobias@ece.gatech.edu, lanterma@ece.gatech.edu

3. SCENARIO CONFIGURATION

The FoV in our simulation consists of an $80\,km \times 80\,km$ stretch of the Washington D.C. area. The receiving antenna is in the middle of the FoV and is assumed to be located on the Lockheed Martin Mission Systems building. We suppose that we are using a receiver such as Lockheed Martin's *Silent Sentry*® system, except with a simpler antenna. The "illuminators of opportunity" consist of three non-cooperative FM transmitters. The transmitter specifications are given in Table 1, and their locations can be seen in Fig. 2(a). The receiver coordinates and system specifications are listed in Table 2. All antennas are assumed to be omni-directional, and thus they have unity gain. The noise figure listed is assumed to be a valid approximation for an urban environment such as Washington D.C.[2]

Table 1. Transmitting antenna specifications.

Call Letters	Latitude	Longitude	Frequency (f)	Power (P_T)
WAMU	38.936 °N	77.093 °W	88.5 MHz	50.0 kW
WETA	38.892 °N	77.132 °W	90.9 MHz	75.0 kW
WPGC	38.864 °N	76.911 °W	95.5 MHz	50.0 kW

Table 2. Receiver system specifications.

Latitude	39.153 °N
Longitude	77.215 °W
Coherent Processing Interval (CPI)	0.5 sec
System Temperature (T_S)	290 K
Noise Figure (NF)	30 dB
Gain (G_R)	0 dB

4. THE PHD-BASED PARTICLE FILTER

Ronald Mahler introduced the concept of a probability hypothesis density, which is defined as being any function that, when integrated over any given area, specifies the expected number of targets present in that area. More specifically, the PHD is the factorial moment density found in point process theory, and it provides a straightforward method of estimating the number of targets in a region under observation. Using probability generating functionals and set calculus, Mahler derives Bayesian time-update and data-update equations that use the PHD to perform motion prediction and incorporate sensor observations, respectively.[3–7]

We use the particle filter implementation of the update equations,[8] whereby the PHD is represented by a collection of particles and their corresponding weights. At time-step k, each particle in our filter is a vector of the form $\xi_i = [x_i\ y_i\ \dot{x}_i\ \dot{y}_i]^T$ and has a weight $w_{i,k}$, where (x_i, y_i) specify the particle's location and $(\dot{x}_i, \dot{y}_i)$ specify its velocity components. As per the defining property of the PHD,

$$N_{k|k} = \sum_i w_{i,k} \tag{2}$$

and

$$\tilde{N} = E[no.\ of\ targets] = [N_{k|k}]_{nearest\ integer.} \tag{3}$$

4.1. Initialization

The simulation starts with 9,000 particles. The particle weights are initialized to zero, since we do not expect any targets to be present at time $k = 0$. This is a different initialization from that of Ref. 1, where it was required to assume that one target was present at $k = 0$. The assumption, however, is unnecessary. Furthermore, any suspected targets can be modelled by using the birth particles in the time-update step.

4.2. Time Update

The time-update step of the particle filter involves propagating each particle by a simple transition constant-velocity matrix and adding uniform process noise. 1,000 birth particles are also added to the time-updated PHD; this is discussed in more detail in Sec. 6.3. Our simulation assumes that targets will not spontaneously disappear, nor will they spawn new targets. The results of the time-update step are the propagated particles and their associated weights, indicated by $\tilde{w}_{i,k+1}$, which represent the predicted PHD for time-step $k + 1$.

4.3. Data Update

In the data-update step, the time-predicted $\tilde{w}_{i,k+1}$ are converted to the final PHD particle weights, $w_{i,k+1}$, by incorporating the radar observations at time k. Given a single sensor with the set of observations $Z_s = \{z_1, ..., z_m\}$ made at time k, probability of detection $p_D(\boldsymbol{\xi})$, single-target likelihood function $f(\mathbf{z}|\boldsymbol{\xi})$, and a Poisson-distributed false alarm rate with parameter λ and density $c(\mathbf{z})$, then the data-updated weights are computed by:

$$w_{i,k+1} = (\sum_{n=1}^{m} u_{i,n}) \; + \; \tilde{w}_{i,k+1}(1 - p_D(\boldsymbol{\xi})) \tag{4}$$

where

$$u_{i,n} = \frac{p_D(\xi_i) f(z_n|\xi_i) \tilde{w}_{i,k+1}}{\lambda c(z_n) \; + \; \sum_{j=1}^{N} p_D(\xi_j) f(z_n|\xi_j) \tilde{w}_{j,k+1}} \tag{5}$$

for $i = 1, \ldots, N$, where N is the total number of particles.

In the bistatic passive radar case, each receiver and transmitter pair constitutes a sensor. Thus, there are three sensors in our configuration, and three sets of range observations are collected at each time step, namely $\{Z_1, Z_2, Z_3\}$. To determine the final weights for this multisensor case, (4) and (5) were first applied to Z_1. The resulting $w_{i,k+1}$ were then used as the $\tilde{w}_{i,k+1}$ to reiterate (4) and (5) over Z_2. The latter procedure was repeated for Z_3 to find the final multisensor particle weights.

Having generated the final particle weights, $w_{i,k+1}$, we compute the expected number of targets in the FoV via (3). The locations of the $\tilde{N}$ expected targets are found by extracting the $\tilde{N}$ highest peaks from the PHD represented by these weights. We have used an EM algorithm for this extraction.[1]

4.4. Resampling

Before iterating the particle filter over the next time step, the particles are resampled via a Monte Carlo method to obtain 9,000 equally weighted particles where

$$\sum_i w_i = \sum_i w_{i,k+1}. \tag{6}$$

5. BISTATIC RADAR VARIABLES

5.1. Signal-to-Noise ratio, SNR

To compute $f(z_n|\xi_i)$ and $p_D(\xi_i)$, it is first necessary to compute each sensor's signal-to-noise ratio for each particle. The SNR is calculated as follows[9, 10]:

$$SNR(\boldsymbol{\xi}) = \frac{K}{R_T^2 R_R^2} \tag{7}$$

where R_T and R_R are as given in (1), and

$$K = \frac{P_T\, G_T\, G_R\, \lambda_f^2\, \sigma_{rcs}\, F_T^2 F_R^2}{(4\pi)^3 k\, T_S(\frac{1}{CPI})(NF)} \tag{8}$$

and $\lambda_f = \frac{c}{f}$, where c is the speed of light, and f is the frequency of the FM signal given in Table 1. The transmitter power (P_T) and transmitter gain (G_T) are also taken from Table 1. The receiver gain (G_R), system noise (T_S), coherent processing interval (CPI), and noise figure (NF) are taken from Table 2. The Boltzmann constant is represented by k, and F_T and F_R are the signal propagation factors. For this study, we assume that signal propagation gains and losses are negligible. The target's bistatic radar cross section is denoted by σ_{rcs}.

5.2. Probability of Detection, p_D

The bistatic radar's probability of detection is calculated based on its SNR and the probability of false alarm, p_{FA}. At low frequencies, the target may reasonably be assumed to be slowly fluctuating; hence, we employ a Rician target model.

$$p_D(\boldsymbol{\xi}) = Q\left[\sqrt{2\,SNR(\boldsymbol{\xi})}\,, \sqrt{2\ln\left(\frac{1}{p_{FA}}\right)}\,\right] \tag{9}$$

where Q is the Marcum Q-function, $SNR(\boldsymbol{\xi})$ is given by (7), and p_{FA} is set to a fixed value.[11] The larger the p_{FA}, the smaller the p_D. For a fixed p_{FA}, a gain in SNR corresponds to an increase in p_D.

In our simulation, we chose $p_{FA} = 10^{-4}$. This allows us to achieve a $p_D = 0.9999$ with an $SNR = 14.94\ dB$, and a $p_D = 0.1$ when $SNR = 6.19\ dB$.[11] For reasonable simulation, p_D was restricted to a maximum value of 0.99999.

Note that the $p_D(\boldsymbol{\xi})$ in (4) does not depend on any specific radar observation, since the $(1 - p_D(\boldsymbol{\xi}))$ term deals with potential missed targets. Thus we must choose a σ_{rcs} that we suppose a potential missed target would have were the radar to detect it. In our simulation, we set $\sigma_{rcs} = 10\ dB$, as we use this value for all our targets.

5.3. Single-Target Likelihood, $f(\mathbf{z}|\boldsymbol{\xi})$

The single-target likelihood function of each bistatic radar antenna pair determines how close each particle's (x, y) values are to the observed target's location, given that the radar observes only the range measurement given by (1). Each particle's corresponding bistatic range measurement is computed (R_{ξ_i}), as well as the difference between it and the observed range.

$f(z_i|\xi_i)$ is a normal density function with mean R_{ξ_i} and variance σ_r^2, where σ_r^2 is the variance of the bistatic range as given by:

$$\sigma_r^2 = \sigma_t^2 \cdot c^2 \tag{10}$$

and[12]

$$\sigma_t^2 = \frac{1}{2\,\beta^2\,SNR(\xi_i)} \tag{11}$$

where β is the transmitter bandwidth, which we take to be $25\ kHz$, and $SNR(\xi_i)$ is given by (7).

5.4. Typical measurements

Table 3 lists ranges of typical values that we have observed for the variables introduced in Sec. 5.

6. OBSERVATIONS

6.1. Simulation Run

Our simulation contains two targets. The first enters at time $k = 7$ at location $(80\,km, 20\,km)$ on our FoV and travels West at $395\,km/hr$ $(190.7\,m/s)$. The second enters at time $k = 9$ from location $(50\,km, 0\,km)$ and travels North at $340\,km/hr$ $(94.4\,m/s)$. They are both assumed to have a $\sigma_{rcs} = 10\ dB$.

The PHD particle filter is seen to identify the correct number of targets present at each time step. Furthermore, the filter correctly ignores the ghost target locations. At present, the EM peak extraction algorithm that was used in Ref. 1 has not yet been fully applied to the current simulation data. However, as can be seen in Fig. 2(b) and Fig. 4, the expected location of the targets can be found at the peaks in the final PHD at each time step.

Table 3. Typical ranges of bistatic radar variables observed in our simulation. See Sec. 6.3 for an explanation of birth particle placement.

Variable	min	max	Birth particle placement
p_D	0.62	0.99999	Uniform
SNR	10 dB	32.5 dB	Uniform
p_D	0.948	0.99999	Targeted clusters
SNR	12.2 dB	32.5 dB	Targeted clusters
σ_r	89 m	1.5 km	-

6.2. Importance of High SNR

Initially, the simulation was run using a receiver noise figure of $45\ dB$ to explore a worst-case scenario. However, this was found to be an inappropriate model of the Washington D.C. scenario, since it produced an SNR which was too low over most of the $80\,km \times 80\,km$ coverage area. With such poor SNR, the p_D was only above 0.9 for the immediate area around the antenna pairs, while most of the FoV had a p_D close to zero (see Fig. 1(a)).

The prevalence of low p_D caused the filter to become unstable. Because the birth particles that were added to the filter in the time-update step were located in an area of low p_D, the $\tilde{w}_{i,k+1}(1 - p_D(\boldsymbol{\xi}))$ term of (4) continually increased at each time step, predicting many targets that did not exist. This makes sense, since the filter can only assume that targets are appearing in the area of low SNR based on the birth particle model. It does not receive any radar observation information to contradict the assumption.

The peak found in the upper-left corner of the PHD shown in Fig. 1(b) is an example of this phenomenon. In the FoV of our simulation, in which the noise figure was reduced to the still reasonable assumption of $30\ dB$, this is the only area that retains a sufficiently low SNR to produce a $p_D < 0.9$.

It is assumed that restricting birth particle placement to regions of high SNR, or simply restricting the FoV to include only regions of sufficiently high SNR, will mitigate the effect of areas of low p_D on the filter.

6.3. Clustered Birth Particles

Birth particles are used in the time-update step of the PHD particle filter (see Sec. 4.2) to represent the PHD of new targets that enter the FoV. Thus, they indicate where new targets are likely to appear at the current time step. Initially, the placement of the birth particles was uniform along the edges of the FoV, as shown in Fig. 3. However, an alternative approach is to use targeted cluster placement of birth particles. Initially designed to economize on the number of particles used, targeted clustering also achieves better target tracking results. Targeted clustering works by placing birth particles in clusters centered at the points where the bistatic range ellipses intersect the edges of the FoV. Each cluster is spread about its center according to a normal distribution with variance equivalent to the variance of a bistatic range cell. The calculation for this bistatic range cell variance is given in Sec. 6.3.1. An example of targeted clustering can be seen in Fig. 2(a). We revert to uniform placement of birth particles around the edges of the FoV when no bistatic ellipses intersect the FoV boundaries. In both placement methods, all 1,000 birth particles are given equal weighting, such that $\sum w_{birth_i} = 1$, since we assume that only one target might enter the FoV at each time step.

Without targeted cluster placement of birth particles, the PHD filter failed to detect one of the targets from time $k = 12$ until $k = 22$. When using targeted clustering, however, both targets were detected and continued to be detected as soon as they appeared. This is to be expected, since by performing targeted cluster placement of the birth particles, we introduced additional prior information into the filter. However, it is assumed that if one were to have the computing resources to simulate with many more particles, then the marginal benefit of targeted clustering would decrease.

6.3.1. Bistatic Range Cells

A bistatic range cell is the resolution at which a bistatic radar can pinpoint a target's location. The bistatic range cell is approximated by[9]:

$$\Delta R_B \approx \frac{c\tau}{2\cos(\frac{\psi}{2})} \tag{12}$$

where τ is the compressed pulse width and ψ is the bistatic angle:

$$\psi = \cos^{-1}\left[\frac{R_T^2 + R_R^2 - L^2}{2R_R R_T}\right] \tag{13}$$

where L is the distance between transmitter and receiver.

Thus,

$$\Delta R_B \approx \frac{c\tau\sqrt{R_R R_T}}{\sqrt{1 + R_T^2 + R_R^2 - L^2}}\,. \tag{14}$$

So,

$$\sigma_{R_B}^2 \approx \frac{c^2\sigma_t^2 R_R R_T}{1 + R_T^2 + R_R^2 - L^2} \tag{15}$$

where σ_t^2 is as given in (11).

Values of σ_{R_B} in our simulation are found to range on the order of $100\,m$ to $550\,m$.

7. CONCLUSIONS AND FUTURE WORK

7.1. Conclusions

The multitarget tracking PHD particle filter, using only bistatic range measurements, was shown to have promise in a simulation designed to mimic a potential real-world scenario. We have found that Mahler's PHD formulation seems to become unstable if one attempts to track targets in regions where the SNR is too low. For computational reasons, we have proposed a targeted cluster placement approach for dealing with the birth particles. This approach has been observed to improve target tracking, given that we are limited in the number of particles we can reasonably use.

7.2. Future Work

Some directions for future work include:

- An expectation-maximization (EM) algorithm was used in Ref. 1 to extract the locations of the peaks of the PHD. This EM algorithm needs to be performed on the current simulation. As shown in Table 4, preliminary results are promising.
- We used bistatic Doppler measurements, in addition to bistatic range, in our original PHD particle filter described in Ref. 1. We are currently implementing this additional source of data in our Washington, D.C. scenario.
- The number of targets appearing and disappearing have yet to be varied, and additional target configurations will be tested. Various flight patterns, including a variety of velocities and accelerations, will also be simulated.
- The effects of interference from the direct-path signal also need to be included in the model.
- Finally, we will introduce coarse direction of arrival measurements into the simulation, as well.

ACKNOWLEDGMENTS

We thank Dr. Ronald Mahler for all of the insightful explanations, comments, and suggestions that he has provided us in our work with the Probability Hypothesis Density.

Table 4. The EM peak extraction algorithm was run on the PHD shown in Fig. 2. The results are provided below. Note that the error between the expected location obtained from the PHD and the true target location is on the same order of magnitude as the bistatic range cell described in Sec. 6.3.1.

Parameter	True (m)	Expected (m)	Error
Target $1, x$	79561.11	79704.50	$143.39\,m$
Target $1, y$	20000.00	19776.02	$-223.98\,m$
Target $2, x$	50000.00	49931.12	$-68.88\,m$
Target $2, y$	189.89	129.20	$-60.69\,m$

REFERENCES

1. M. Tobias, "A probability hypothesis density-based multitarget tracker using multiple bistatic range and velocity measurements," in *Proc. of the 36th Southeastern Symposium on System Theory*, pp. 205–209, (Atlanta, GA), March 2004.
2. L. M. Ehrman, "Automated target recognition using passive radar and a coordinated flight model," Master's thesis, Georgia Institute of Technology, Atlanta, Georgia, May 2004.
3. R. Mahler, "Multitarget moments and their application to multitarget tracking," in *Proc. of The Workshop on Estimation, Tracking, and Fusion: A Tribute to Yaakov Bar-Shalom*, pp. 134–166, (Monterey, CA), May 2001.
4. R. Mahler and T. Zajic, "Multitarget filtering using a multitarget first-order moment statistic," in *Signal Processing, Sensor Fusion, and Target Recognition X*, I. Kadar, ed., **SPIE Proc. 4380**, pp. 184–195, 2001.
5. A. El-Fallah, T. Zajic, R. Mahler, B. Lajza-Rooks, and R. Mehra, "Multitarget nonlinear filtering based on spectral compression and probability hypothesis density," in *Signal Processing, Sensor Fusion, and Target Recognition X*, I. Kadar, ed., **SPIE Proc. 4380**, pp. 207–216, 2001.
6. R. Mahler, "Objective functions for bayesian control-theoretic sensor management, i: Multitarget first-moment approximation," in *Proc. of IEEE Aerospace Conference*, **4**, pp. 1905–1924, (Big Sky, MT), March 2003.
7. R. P. S. Mahler, "Multitarget bayes filtering via first-order multitarget moments," in *IEEE Trans. Aerospace and Electronic Systems*, **39**(4), pp. 1152–1178, 2003.
8. T. Zajic and R. Mahler, "A particle-systems implementation of the phd multitarget tracking filter," in *Signal Processing, Sensor Fusion, and Target Recognition XII*, I. Kadar, ed., **SPIE Proc. 5096**, pp. 291–299, 2003.
9. N. Willis, *Bistatic Radar*, Technology Service Corporation, 1995.
10. P. E. Howland, *Television Based Bistatic Radar*. PhD thesis, University of Birmingham, ENGLAND, 1997.
11. B. Mahafza, *Introduction to Radar Analysis*, CRC Press LLC, 1998.
12. D. Barton, *Modern Radar System Analysis*, Artech House, Inc., 1988.

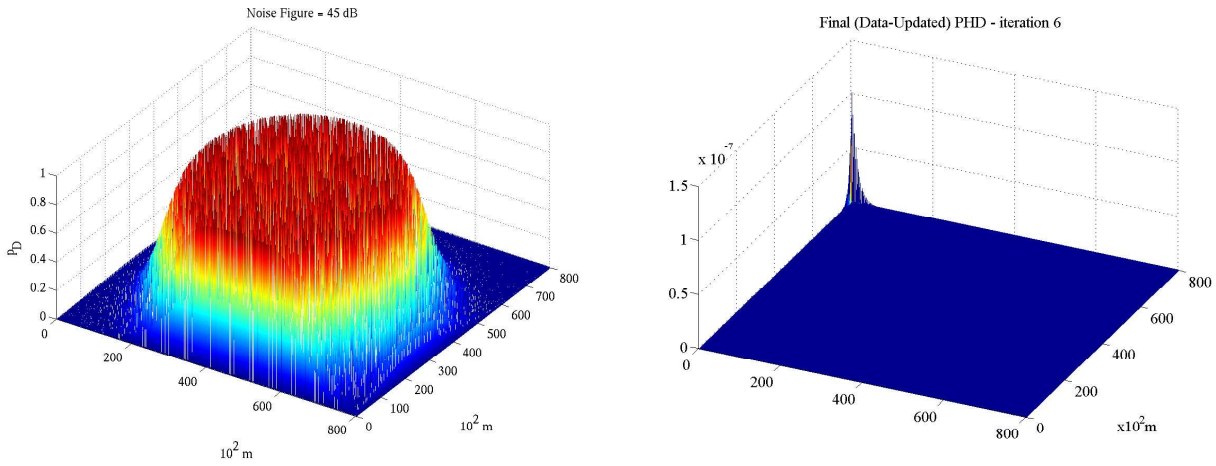

(a) (b)

Figure 1. These figures indicate the importance of SNR in the simulation. Figure 1(a) indicates the probability of detection when the noise figure of the receiver is $45\,dB$. Note that most of the field of view (FoV) has a $p_D < 0.6$. When the noise figure is reduced to $30\,dB$, the SNR increases, and the area of low p_D is confined to the far upper-left corner of the FoV. It's effect on the PHD in the absence of targets is shown in Fig. 1(b).

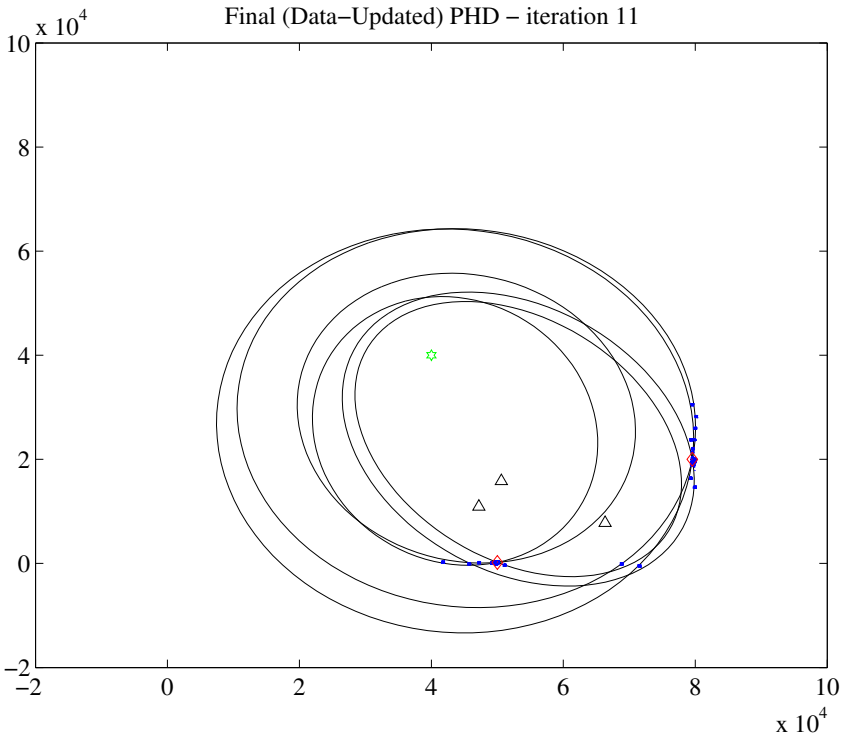

(a) The PHD particle filter and range ellipses. The hexagon represents the location of the receiving antenna, and the triangles represent the transmitting antennas. Target positions are indicated by diamonds. Each particle of the filter is pictured. Note the targeted cluster placement of birth particles.

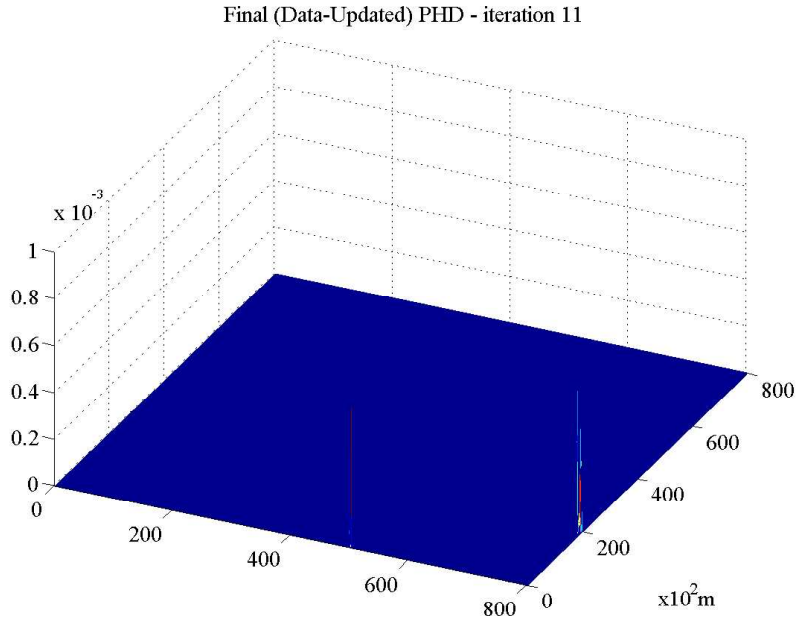

(b) The particle weights of the PHD filter. The sum of the weights is 1.765.

Figure 2. The PHD particle filter at time $k = 11$.

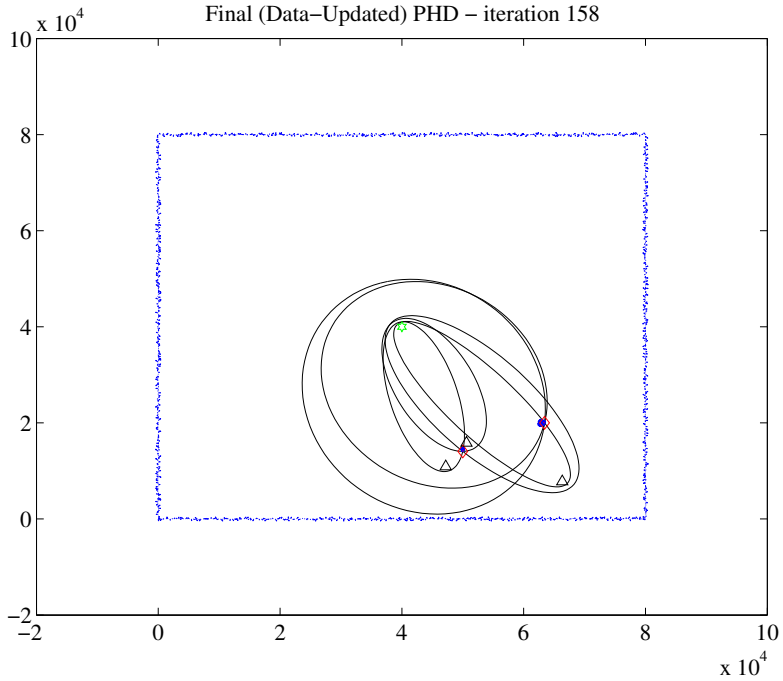

Figure 3. The PHD particle filter at time $k = 158$. Note the uniform placement of birth particles, which appear as a rectangle along the edge of the FoV, since none of the bistatic range ellipses intersect the FoV boundaries. Note also that all ghost targets have vanished.

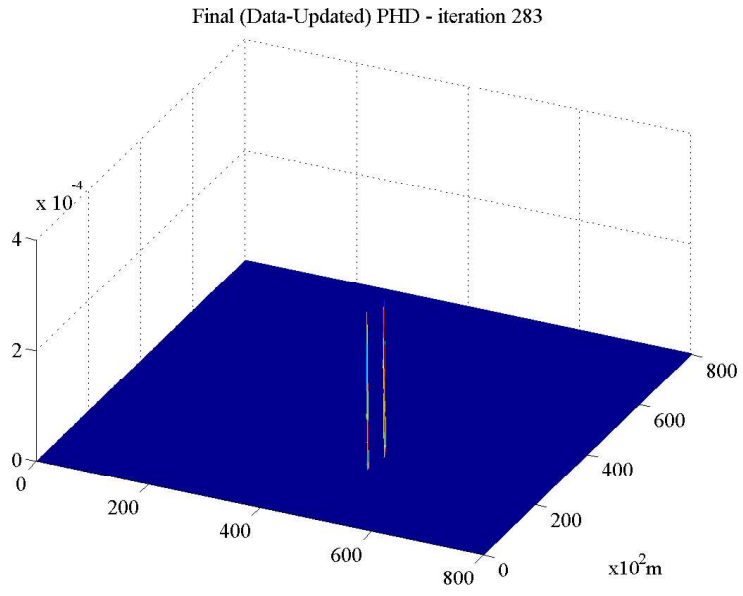

Figure 4. The PHD particle filter at time $k = 283$, after the targets' paths have crossed. The sum of the particle weights is 1.940.